Inorganic Chemistry

Article

pubs.acs.org/IC

Structural and Electronic Dependence of the Single-Molecule-Magnet Behavior of Dysprosium(III) Complexes

Victoria E. Campbell,*[,†] Hélène Bolvin,[‡] Eric Rivière,[†] Regis Guillot,[†] Wolfgang Wernsdorfer,[§] and Talal Mallah*[,†]

[†]ICMMO, Université de Paris Sud, 15 rue Georges Clemenceau, 91405 Orsay, France

[‡]Laboratiore de Chimie et Physique Quantiques, Université Toulouse III, 118 route de Narbonne, 31062 Toulouse, France

[§]Department of Nanoscience, Insitut Néel, 25 rue des Martyrs, 38042 Grenoble, France

Supporting Information

ABSTRACT: We investigate and compare the magnetic properties of two isostructural Dy^{III}-containing complexes. The Dy^{III} ions are chelated by hexadentate ligands and possess two apical bidendate nitrate anions. In dysprosium(III) *N*,*N*′-bis(imine-2-yl)methylene-1,8-diamino-3,6-dioxaoctane (**1**), the ligand's donor atoms are two alkoxo, two pyridine, and two imine nitrogen atoms. Dysprosium(III) *N*,*N*′-bis(amine-2-yl)methylene-1,8-diamino-3,6-dioxaoctane (**2**) is identical with **1** except for one modification: the two imine groups have been replaced by amine groups. This change has a minute effect on the structure and a larger effect the magnetic behavior. The two complexes possess slow relaxation of the magnetization in the presence of an applied field of 1000 Oe but with a larger barrier for reorientation of the magnetization for **1** (U_{eff}/k_B = 50 K) than for **2** (U_{eff}/k_B = 34 K). First-principles calculations using the spin−orbit complete active-space self-consistent-field method were performed and allowed to fit the experimental magnetization data. The calculations gave the energy spectrum of the $2J + 1$ sublevels issued from the $J = {}^{15}/_{2}$ free-ion ground state. The lowest-lying sublevels were found to have a large contribution of $M_J = \pm{}^{15}/_{2}$ for **1**, while for **2**, $M_J = \pm{}^{13}/_{2}$ was dominant. The observed differences were attributed to a synergistic effect between the electron density of the ligand and the small structural changes provoked by a slight alteration of the coordination environment. It was observed that the stronger ligand field (imine) resulted in complex **1** with a larger energy barrier for reorientation of the magnetization than **2**.

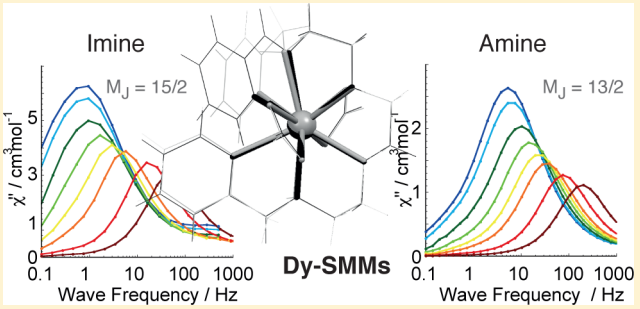

INTRODUCTION

Magnets have fascinated scientists for centuries and are at the center of many technological advances.[1] Since their discovery in the 1990s,[2] single-molecule magnets (SMMs) have been the focus of extensive research. The interest for these kinds of molecules lies in their magnetic bistability. It was shown that, at low temperatures (liquid-helium range), even in the absence of an external magnetic field, SMMs retain magnetization over long periods.[3] This bistability is observed in molecules that possess a large spin (S) ground state in addition to large Ising-type magnetic anisotropy (negative zero-field-splitting parameter D) for the spin Hamiltonian $DS_z^2 - S(S + 1)/3$. The energy barrier of reorientation of the magnetization (U) is $U = S^2|D|$ and $(S^2 - 1/4)|D|$ for integer and half-integer spin systems, respectively. Therefore, to increase U_{eff} and consequently increase its temperature of operation, it is possible to increase either S or D or both. The strategy employed for first-generation SMMs was to assemble large clusters that had high-spin ground states. The classic example is the famous dodecametallic manganese acetate family of SMMs ($Mn_{12}Ac$), which have S = 10 and U_{eff} up to 74 K.[4] However, the increase of the total spin has yielded a decrease in the total anisotropy of these systems. For example, Christou et al. reported a transition-metal complex that had a record barrier (U_{eff} = 86 K) but a $|D|$ parameter of 0.62 K (down from 2.0 K).[5]

In order to render SMMs that are attractive as potential new materials for quantum information devices that use spins to manipulate or store information,[6] it is essential to design and synthesize SMMs that function at higher temperatures. Therefore, in the past decade, strategies that employ metals with large orbital angular momenta, such as lanthanides and actinides, have been successfully employed.[7] In the pursuit for new SMMs, the most remarkable results have been obtained with lanthanide coordination compounds.[8] For example, Winpenny and co-workers reported a polynuclear SMM that exhibited record barriers of U_{eff} = 528 K in undiluted samples and U_{eff} > 800 K for magnetically diluted samples.[9] Furthermore, slow relaxation in Ln-SMMs may be observed in single-lanthanide-ion complexes. Very large energy barriers

Received: November 28, 2013
Published: February 17, 2014

   dx.doi.org/10.1021/ic402950j | *Inorg. Chem.* 2014, 53, 2598−2605

of reorientation of the magnetization were reported for phthalocyanin (Pc) double-decker complexes of terbium(III) and dysprosium(III)[10] and for an erbium(III) ion sandwiched between polyoxometallate ligands.[11]

Among the lanthanides, the largest number of pure Ln-SMMs has been achieved with dysprosium(III).[12] This phenomenon may be explained by the high moment and high anisotropy of the dysprosium(III) ion, which has a half-integer ground state (for the free ion: $^6H_{15/2}$ and $g = {}^4/_3$), leading to low-lying Kramers doublets and consequently to reduced predisposition in dysprosium(III) systems to show quantum tunneling of the magnetization (QTM). The synthetic strategy employed thus far is similar to that used for the construction of transition-metal SMMs and has relied on the synthesis of polydentade ligands followed by lanthanide-ion complexation. The ligand field lifts the degeneracy of the $2J + 1$ sublevels. This, in turn, may result in a ground state that has $m_J = \pm J$, generating large Ising-type magnetic anisotropy.[13] Even though theoretical calculations allow for determination of the nature of the ground state and thus consent a satisfactory interpretation of the magnetic behavior, the influence of the chemical parameters on the magnetic properties is still unclear. Therefore, the study of smaller systems is crucial for understanding the rules that direct the overall anisotropy and magnetic properties of Ln-SMMs.

To the best of our knowledge, previous studies have mostly focused on either changing the lanthanide ion while keeping the ligand system constant[10,12a,e,g,13,14] or changing the ligand but keeping the coordination sphere around the lanthanide ion identical in multilanthanide systems.[12b,15] In a study by Ishikawa and co-workers, protonation of the ligand resulted in the switching of the SMM properties of the terbium double-decker molecule.[16] This behavior was attributed to the loss of D_{4d} symmetry caused by deprotonation. Furthermore, the electrostatic environment around the lanthanide ion changed between the protonated and deprotonated states. In a recent study by Murugesu and co-workers, the effects of electron-withdrawing groups on the energy barrier in dinuclear dysprosium(III) SMMs were investigated. It was found that, by a change in the electronic properties of the ligands situated in the equatorial position with respect to the anisotropy axis, a drastic increase in the energy barrier of the magnetization could be observed.[17] In the quest to better understand these rules, herein, we investigate and compare the magnetic properties of two dysprosium(III)-containing complexes. A small modification in the ligand resulted in the synthesis of two isostructural mononuclear dysprosium(III) compounds, which have different magnetic behaviors. In this system, the charge and coordination geometry around the dysprosium(III) ion does not change between the two complexes. The observed magnetic data are correctly reproduced by first-principles calculations, which indicated that the magnetic moments of the ground Kramers doublet are different in the two complexes. These differences are attributed to a synergistic effect between the coordination geometry, which is almost identical in the two complexes, and the electronic nature of the donor atoms.

EXPERIMENTAL SECTION

General Procedures. All reactions were carried out in a 20 mL scintillation vial. Unless otherwise stated, all reagents were purchased from Aldrich or TCI and used without further purification. Methanol (MeOH) was dried by distillation over calcium hydride. The complex dysprosium(III) *N,N′*-bis(imine-2-yl)methylene-1,8-diamino-3,6-dioxaoctane (**1**) was synthesized according to literature procedures.[12e] *N,N′*-Bis(imine-2-yl)methylene-1,8-diamino-3,6-dioxaoctane (LH_2) was synthesized according to modified literature procedures.[18] Electrospray ionization mass spectrometry (ESI-MS) spectra were recorded on a Thermo Scientific 2009 mass spectrometer. NMR spectra were recorded on a Bruker Aspect 300 NMR spectrometer. IR spectra were recorded on a Bruker TENSOR-27 Fourier transform infrared (FT-IR) spectrometer equipped with an attenuated total reflectance (ATR crystal diamond/ZnSe) sample holder in the 4000−500 cm^{-1} range. Elemental analysis was taken on a Thermo Scientific Flash analyzer.

Synthesis of Dysprosium(III) *N,N′*-Bis(amine-2-yl)methylene-1,8-diamino-3,6-dioxaoctane (2). To a 20 mL scintillation vial were added LH_2 (85.6 mg, 0.26 mmol) and 5 mL of dry MeOH with stirring at 323 K for 5 min. To this solution was added dropwise a solution of $Dy(NO_3)_3{\cdot}5H_2O$ (113.6 mg, 0.26 mmol) in 1 mL of dry MeOH, and the solution was left at 323 K for 3 h. The product was purified by vapor diffusion of Et_2O into a MeOH solution of **2** (m = 0.112 g; yield = 80%). IR (ν/cm^{-1}): 3317 (br), 2946 (br), 2888 (br), 2529 (br), 2162 (s), 1981 (br), 1780 (m), 1660 (s), 1626 (m), 1589 (m), 1571 (m), 1469 (br), 1446 (s), 1366 (br), 1352 (br), 1286 (s), 1226 (s), 1156 (s), 1104 (m), 1091 (m), 1051 (m), 1033 (m), 1010 (s), 988 (s), 962 (m), 937 (s), 897 (s), 875 (s), 813 (m), 785 (m), 744 (m), 707 (br), 662 (s), 634 (m). ESI-MS: m/z 309.05 ($[\mathbf{2}]^{2+}$). Elem anal. Calcd for $C_{19}H_{34}N_7O_{14}Dy$ ($C_{19}H_{34}N_7O_{14}Dy$): C, 30.55; H, 4.59; N, 13.10. Found: C, 30.70; H, 4.33; N, 13.25.

Single-Crystal X-ray Diffraction Studies. X-ray diffraction data were collected by using a Bruker Kappa X8 APEX II diffractometer with graphite-monochromated Mo Kα radiation (λ = 0.71073 Å). Crystals were mounted on a CryoLoop (Hampton Research) with paratone-N (Hampton Research) as the cryoprotectant and then flash frozen in a nitrogen-gas stream at 100 K. The temperature of the crystal was maintained at the selected value (100 K) by means of a Cryostream 700 series cooling device to within an accuracy of ±1 K. The data were corrected for Lorentz polarization and absorption effects. The structures were solved by direct methods using *SHELXS-97*[19] and refined against F^2 by full-matrix least-squares techniques using *SHELXL-97*[20] with anisotropic displacement parameters for all non-hydrogen atoms. Hydrogen atoms were located on a difference Fourier map and introduced into the calculations as a riding model with isotropic thermal parameters. All calculations were performed using the Crystal Structure crystallographic software package *WINGX*.[21] The crystal data collection and refinement parameters are given in Table S1 in the Supporting Information (SI).

Magnetic Measurements. The magnetic susceptibility measurements were obtained using a Quantum Design SQUID MPMS-XL7 magnetometer operating between 1.8 and 300 K for direct-current (dc) applied fields ranging from −7 to +7 T. dc analysis was performed on polycrystalline samples of **1** and **2** (17.61 and 17.31 mg, respectively) wrapped in eicosan under a field between 0.1 and 1 T and between 1.8 and 300 K. Alternating-current (ac) susceptibility measurements were carried out under an oscillating field of 1.5 or 3 Oe and ac frequencies ranging between 0.1 and 1500 Hz. Diamagnetic corrections were applied for the sample holder and eicosan.

Micro-SQUID Measurements. Magnetization measurements on oriented single crystals were carried out with an array of micro-SQUIDs.[22] This magnetometer works in the temperature range of 0.04−7 K and in fields of up to 0.8 T with sweeping rates as high as 0.28 T s^{-1} and exhibits field stability of better than mT. The time resolution is approximately 1 ms. The field can be applied in any direction of the micro-SQUID plane with precision greater than 0.1° by separately driving three orthogonal coils. In order to ensure good thermalization, a single crystal was fixed with apiezon grease.

RESULTS AND DISCUSSION

Synthesis. The one-pot reaction between 2-formylpyridine (2 equiv) and 1,8-diamino-3,6-dioxaoctane (1 equiv) with $Dy(NO_3)_3{\cdot}6H_2O$ (1 equiv) in MeOH afforded **1** ($C_{18}H_{22}N_6O_8Dy$; Scheme 1).[12e] We reasoned that synthesizing

dx.doi.org/10.1021/ic402950j | Inorg. Chem. 2014, 53, 2598−2605

Scheme 1. Schematic Representation of the Synthesis of Complexes 1 and 2

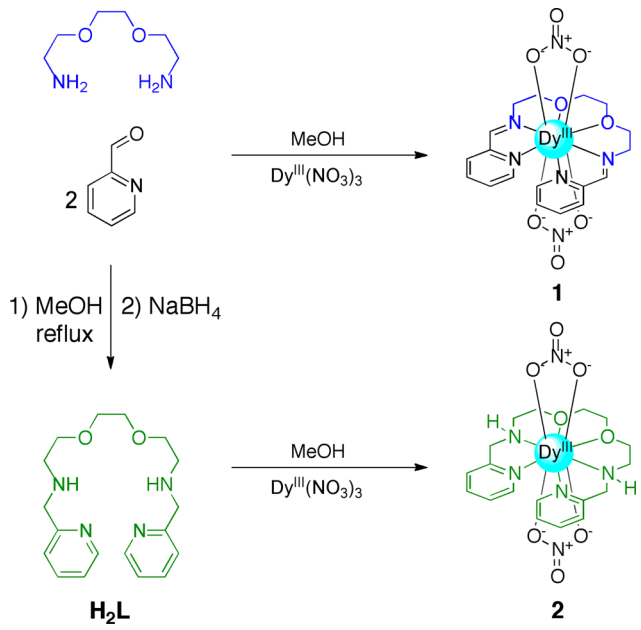

a series of ligands that have different electronic properties would lead to the synthesis of complexes with geometrical conformations similar to those of **1** but with different magnetic behaviors. Therefore, amine-containing ligand H_2L was synthesized via standard imine reduction chemistry and subsequently reacted with $Dy(NO_3)_3{\cdot}6H_2O$ (1 equiv) in MeOH to afford **2** ($C_{18}H_{26}N_6O_8Dy$; Scheme 1).

Both **1** and **2** were purified by recrystallization from diethyl ether, affording off-white X-ray-quality crystals. ESI-MS peaks at m/z 614.05 ($[\mathbf{1}]^+$) and m/z 618.19 ($[\mathbf{2}]^+$) confirmed the presence of **1** and **2** in solution. Further confirmation of complex formation was given by the FT-IR spectra (see the SI), which indicated the presence of the C═N band at 1625 cm^{-1} for **1** and the N−H stretch at 3300 cm^{-1} for **2**.

Crystal Structures. Single-crystal X-ray analysis of **1** and **2** revealed that both complexes crystallized in the triclinic $P\bar{1}$ space group and are isostructural. Shown in Figure 1 is the overlap of the two structures, in which it is possible to better visualize the slight differences between **1** and **2**. In both **1** and **2**, the central dysprosium(III) ion is coordinated to four nitrogen atoms and six oxygen atoms with Dy−N bonds of 2.483−2.585 Å and Dy−O bonds of 2.460−2.561 Å. As expected, the amine N2−Dy (or N3−Dy) bonds are 3% longer than the imine N2−Dy (or N3−Dy) bonds (Table 1). The ligands arrange around the dysprosium(III) ion in a similar fashion. Two oxygen (O1 and O2) and two nitrogen (N2 and N3) atoms are arranged in the equatorial plane around the dysprosium(III) ion. Because of the steric bulk of the pyridine rings (Py1 and Py2), N1 and N2 are twisted out of this mean plane. The dihedral angles between the planes formed by Py1 and Py2 are 57° and 66° for **1** and **2**, respectively (Figure 1). Two nitrate ions contribute four of the donor atoms. The charge balance is given by one nitrate counterion, and there is one molecule of MeOH in the crystal lattice. Analysis of the packing arrangement reveals that there are no strong intermolecular forces between neighboring molecules (such as hydrogen bonds and $\pi-\pi$ stacking) and that the closest distance between dysprosium(III) ions is 8.1 Å.

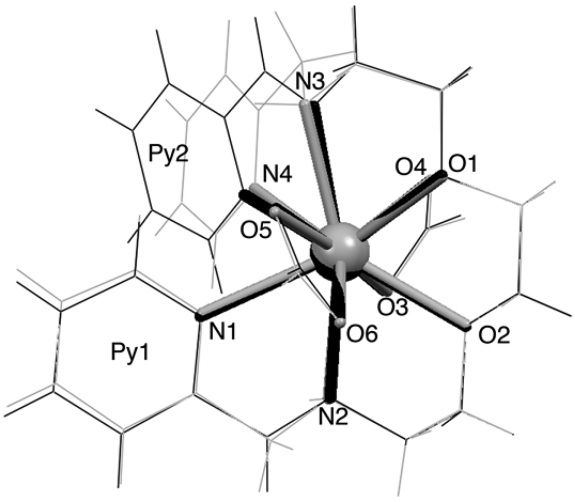

Figure 1. X-ray crystal structure of complexes **1** (black) and **2** (gray). The figure was obtained by overlaying O1 and O2. Solvent molecules and counterions are omitted for clarity.

Table 1. Selected Bond Distances (Å)

1		2	
Dy−N1	2.585(3)	Dy−N1	2.5575(15)
Dy−N2	2.483(4)	Dy−N2	2.5541(13)
Dy−N3	2.503(3)	Dy−N3	2.5438(14)
Dy−N4	2.552(3)	Dy−N4	2.5502(13)
Dy−O1	2.493(3)	Dy−O1	2.4669(11)
Dy−O2	2.478(3)	Dy−O2	2.4601(12)
Dy−O3	2.540(3)	Dy−O3	2.5614(12)
Dy−O4	2.455(3)	Dy−O4	2.4649(12)
Dy−O5	2.490(3)	Dy−O5	2.5256(13)
Dy−O6	2.430(3)	Dy−O6	2.4786(12)

The structural differences between **1** and **2** were investigated because it was shown that the geometry around the lanthanide ion greatly influences the magnetic properties of the resulting complexes.[8b,12h] The two structures differ slightly in the coordination environment; therefore, to better appreciate the differences, **1** and **2** were overlaid at the O1 and O2 positions (Figure 1). Thus, it is possible to see that only small differences in the positions of the donor atoms arise at the N3 and N4 positions. All but two (N1 and N2) of the 10 donor atoms are identical, with the main difference being the strength of the ligand field (electronic properties) of the nitrogen (imine being stronger than amine) atoms. The stronger ligand field resulted in a complex (**1**) that displayed (i) a larger energy difference between the ground state and first excited state and (ii) a dominant contribution to the ground state of the $M_J = \pm{}^{15}/_2$ over the $M_J = \pm{}^{13}/_2$, while the reverse occurs for **2**. These results directly translate to a larger energy barrier of reorientation of the magnetization for **1** than for **2**.

The lanthanide inner-coordination spheres of **1** and **2** resemble each other and are far from an idealized geometry. The closest description may be portrayed as a distorted bicapped square antiprism (Figure 2).). The first deviation from an idealized geometry arises because the atoms do not form a square but a trapezoid. Two trapezoids are defined by the mean planes through four of the coordinating atoms (O1, O4, N4, O5 and O3, O2, N1, O6). The two trapezoids are twisted at skew angles of φ = 58° (**1**) and 40° (**2**) with respect to one another (Figure 2). This angle is far from the expected value for

dx.doi.org/10.1021/ic402950j | Inorg. Chem. 2014, 53, 2598−2605

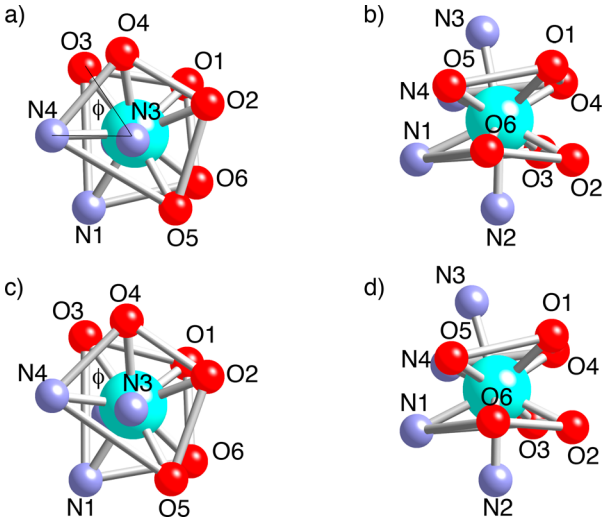

Figure 2. Perspective showing the distorted bicapped square-antiprismatic geometries of the central dysprosium(III) ion for **1** (a and b) and **2** (c and d).

an ideal D_{4d} symmetry (φ = 45°). The second deviation arises from the dihedral angle between the two mean planes, which are at 10° (**1**) and 9° (**2**) with respect to one another.

Magnetic Properties. Magnetic susceptibility measurements for **1** and **2** were carried out under dc applied field between 2 and 300 K at 1000 and 10000 Oe (Figures 3 and 4).

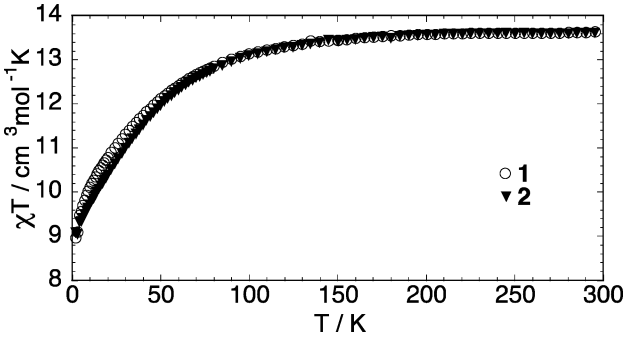

Figure 3. Temperature dependence of the χT product at 1000 Oe (1.8−150 K) and 10000 Oe (150−300 K).

At room temperature, the values of $\chi_M T$ are 13.71 cm^3 mol^{-1} K for **1** and 13.62 cm^3 mol^{-1} K for **2**, which are in good agreement with the expected values for mononuclear dysprosium(III) complexes ($^6H_{15/2}$, $g = {}^4/_3$, and $\chi_M T_{\text{free ion}}$ = 14.17).[23] $\chi_M T$ decreases gradually and then more rapidly below 50 K, which is most likely due to crystal-field effects (thermal depopulation of the M_J sublevels (stemming from the $J = {}^{15}/_2$ ground state). The magnetization (M) versus field (H) plots show that the field dependence of the magnetization does not saturate at the highest available fields and the corresponding $M = f(H/T)$ curves do not superimpose. M reaches at H = 7 T a value close to 5.2 μ_B, much weaker than that expected for saturation (gJ = 10 μ_B). This behavior is indicative of highly magnetically anisotropic complexes.[24]

Dynamic Magnetic Properties. Dynamic magnetic measurements were carried out on complexes **1** and **2**, and a frequency dependence of the out-of-phase susceptibility (χ'') was observed for both systems. It has been previously reported that **1** showed a frequency dependence of χ'' under zero dc

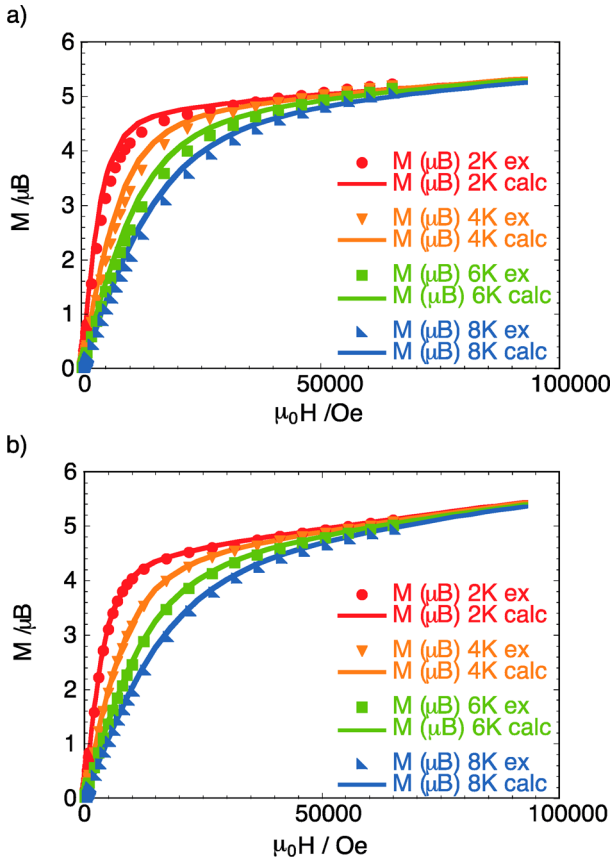

Figure 4. Field dependence of the magnetization at variable temperatures for **1** (top) and **2** (bottom). The solid lines correspond to the SO-CASSCF fits.

applied field, which is indicative of SMM behavior, and that **1** undergoes slow relaxation of the magnetization below 10 K.[12e] To probe the potential SMM behavior of **2**, ac magnetic susceptibility measurements were also carried out in the absence of a dc applied field. Similar to **1**, **2** also undergoes slow relaxation of the magnetization; however, no maximum for χ'' was seen in either complex at the frequency and temperature ranges studied ($T \geq 2$ and $\nu \leq 1500$ Hz). This behavior is frequently reported for lanthanide-containing complexes and may be attributed to small energy barriers stemming from QTM.[15,25] QTM occurs when states are brought into resonance because of the matching of energy levels at zero field and/or under an appropriate magnetic field. It is common for full-integer spin systems to show QTM. However, QTM should not be observed in half-integer spin systems according to Kramers' spin-parity theorem,[26] which dictates that no matter how asymmetric the crystal field, ions with an odd number of electrons have to have at least a doubly degenerate ground state. Therefore, a perturbation that lifts this degeneracy has to be present in order to render QTM possible in our system. Similarly to what was reported by Ishikawa and Wernsdorfer, it is reasonable to say that QTM in the case of dysprosium(III) is occurring between entangle states of nuclear and electronic spins.[14a] Additionally, tunneling may be induced by dipolar coupling and small exchange interactions between molecules.[27]

In order to bypass QTM, ac susceptibility measurements may be carried out under a small optimized dc field, which causes a shift in the maxima of the $\chi'' = f(T)$ curves toward higher

dx.doi.org/10.1021/ic402950j | Inorg. Chem. 2014, 53, 2598−2605

temperatures (Figure 5). The optimal dc field is the field at which the minimum characteristic frequency is observed and

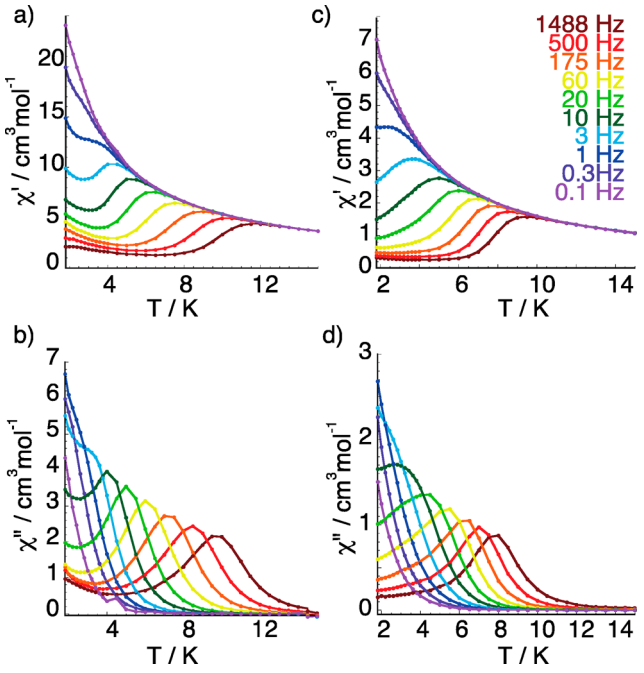

Figure 5. ac susceptibility data for complexes **1** (a and b) and **2** (c and d). Plots of χ' (a and c) and χ'' (b and d) versus temperature at different wave frequencies under a dc field (H = 1000 Oe).

was found to be 1000 Oe for **1**.[12e] Because we are comparing **1** and **2**, this external field was kept constant for a better comparison. Maxima of 9.7 and 8.0 K were observed, at the aforementioned dc field, for a frequency of 1500 Hz for **1** and **2**, respectively.

For both complexes, the relaxation time shows two distinct regimes stemming from a temperature-independent quantum tunneling regime at low temperatures and a temperature-dependent thermally activated regime at temperatures above 5 K. This high-temperature regime follows the Arrhenius law $\tau = \tau_0 \exp(U_{eff}/k_BT)$. It is possible to extrapolate values for the energy barrier of the magnetization (U_{eff}) and the preexponential factor (τ_0) by plotting the magnetization relaxation times (τ) obtained from the ac data as ln τ versus $1/T$. In accordance with the ac data and the first-principles calculations, different U_{eff} and τ_0 values were found for **1** (50 K, 6.80×10^{-7} s) and **2** (34 K, 2.51×10^{-6} s). **2** has a lower energy barrier of the magnetization. These values are comparable to those reported in other mononuclear dysprosium(III) systems. For example, U_{eff}/k_B = 60 K was found for a Dy/DOTA system[28] and U_{eff}/k_B = 23 K for a dysprosium macrocycle.[29]

Semicircular Cole–Cole plots[30] were obtained for both **1** and **2** at temperatures ranging from 1.8 to 6.0 K (Figure 6). The plots for complex **2** showed only one relaxation pathway, while those for **1** indicated the appearance of the beginning of a second relaxation mechanism at low temperature. Only one part of this semicircle was fitted using a generalized Debye model. Analysis revealed that the α parameter is close to zero at higher temperatures, indicating a single relaxation process, while at low temperatures (tunneling regime), for both complexes, α varies between 0.2 and 0.4, which is consistent with previously reported values and suggests that in the tunneling regime the system is more sensitive to strain.[28]

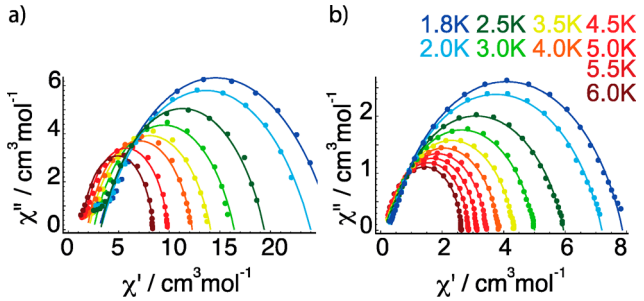

Figure 6. Cole–Cole plots obtained for complexes **1** (a) and **2** (b). The solid lines represent the fit obtained with a generalized Debye model.

In order to test the influence of inter- and intramolecular exchange on the magnetic behavior, we investigated the effect of magnetic dilution on relaxation of the magnetization of **1** and **2**. For this, we cocrystallized a sample in which the dysprosium(III) complex was magnetically diluted with the isostructural yttrium(III) analogue in a molar ratio of 1:10. Dynamic magnetic measurements were carried out on these diluted samples (see the SI). No significant differences were seen between the energy barriers of relaxation of the magnetization of these diluted samples compared to the undiluted ones. Therefore, we may conclude that intermolecular forces and dipolar interactions are negligible at the temperatures studied (>1.8 K).

The slight difference in coordination of the ligand field affected the overall magnetic properties of the complexes. To further probe into the differences in the SMM behavior of **1** and **2** and to gain further insight into their low-temperature behavior, single-crystal magnetization measurements were performed using a micro-SQUID[22] instrument at temperatures ranging from 0.03 to 5 K. The field was aligned parallel to the easy axis of magnetization by the transverse field method.[31] For both complexes, hysteresis loops (Figure 7) were observed and have steplike features, which is indicative of QTM (see the SI for expanded graphs).[9b,14a,27] Each step represents a level where tunneling may occur. The system shows a strong sweep rate dependence. The coercive field increases with increasing temperature (between 0.03 and 0.5 K). Typically, the coercivity of the hysteresis loops increases with decreasing temperature and increasing sweep rate; however, in SMM with a strong tunneling rate at H = 0, this behavior is inverted. At low temperatures, most of the molecules tunnel when the field is swept over the zero-field level crossing.[2b] At high temperatures, the net tunneling rate is reduced by thermally assisted relaxation/excitation near zero field and hysteresis is observed.

Theoretical Calculations. Small modifications in the ligand field have been known to greatly influence the overall magnetic properties of the resulting SMM molecules.[12a,32] In order to gain insight into the observed magnetic properties and into the nature of the ground state of the complexes, first-principles calculations were performed.

The excited states of the complexes have been calculated with the spin–orbit complete active-space self-consistent field (SO-CASSCF) method using the *MOLCAS76* suite of programs.[33] ANO-RCC basis sets of DZP quality were used. The active space included all nine 4f electrons of the dysprosium(III) ion spanning seven orbitals. First, a CASSCF calculation is performed.[34] Second, the spin–orbit is evaluated

dx.doi.org/10.1021/ic402950j | *Inorg. Chem.* 2014, 53, 2598–2605

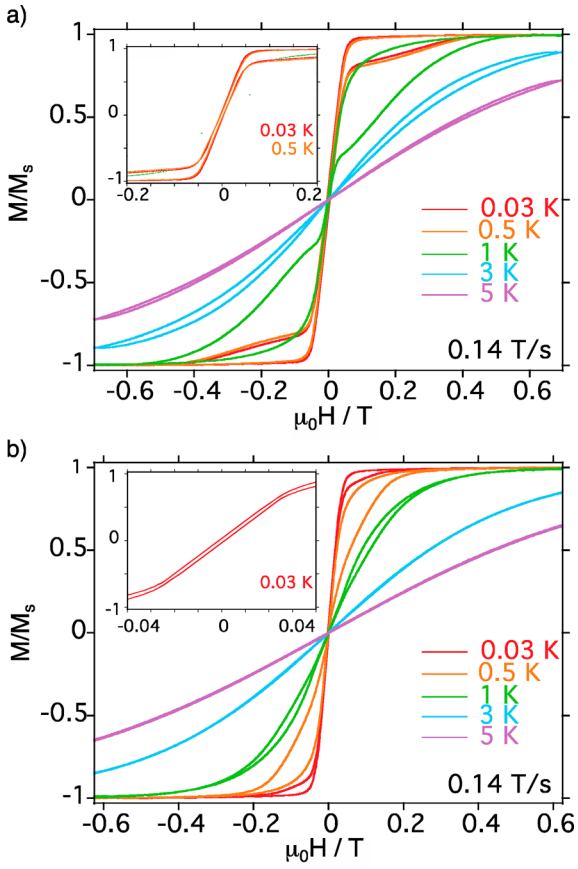

Figure 7. Hysteresis loops for complexes **1** (a) and **2** (b).

by a state interaction[35] and the g factors are calculated by a method previously described by Bolvin.[36]

The obtained energy gaps for the first nine Kramers doublets for **1**–**3** are listed in Table 2. The first eight are derived from the $^6H_{15/2}$ atomic term and the ninth from the $^6H_{13/2}$ one. Because of the low symmetry of the molecules, M_J is not a good quantum number. However, from the values of the g factors of the ground state, it appears that the ground-state doublet may best be described as $|J = {}^{15}/_2, M_J = {}^{15}/_2\rangle$ for **1** ($g_{ax} = 20$) and $|J = {}^{15}/_2, M_J = {}^{13}/_2\rangle$ for **2** ($g_{ax} = 17.3$), which is consistent with the different experimental values of the magnetization observed. The calculated and observed values of the molar magnetization and the values for χT for **1** and **2** at different temperatures (2–8 K) and fields (1000 and 10000 Oe) are shown in Figures 4 and S6 in the SI, respectively. The calculated and observed values are in excellent agreement.

Table 2. Energies of the Lowest Nine Kramers Doublets and the Main Component of the g Factors of the Ground State for Complexes 1 and 2

doublet/DE (cm^{-1})	1	2
1	0.0	0.0
2	95.0	84.7
3	112.1	96.7
4	158.2	121.1
5	277.1	211.8
6	309.0	241.8
7	423.8	319.3
8	450.9	351.7
9	3046.4	3051.6
g_1	18.1	16.9
g_2	0.1	0.4
g_3	0.0	0.3

The energies of the first excited Kramers doublet (95.0 cm^{-1} for **1** and 84.7 cm^{-1} for **2**) are on the same order of magnitude as the values corresponding to the experimental values of the barrier for reorientation of the magnetization (50 and 34 K for **1** and **2**, respectively). These values of the **g** tensor are listed in Table 2. The calculations gave larger transverse components (g_x and g_y) for **2** than for **1**. Furthermore, for complex **1**, the g_z component of the **g** tensor more closely resembles that of the Kramers doublet of a pure $|J = {}^{15}/_2, M_J = {}^{15}/_2\rangle$ ($g_z = 20$) and for **2** that of a pure $|J = {}^{15}/_2, M_J = {}^{13}/_2\rangle$ ($g_z = 17.3$).[37] The larger g_z value for **1** indicates a larger magnetic anisotropy for **1** than for **2** and is consistent with the experimental data that show a larger anisotropy barrier for **1** than for **2**. It is possible to determine the orientation of the anisotropy axes from first-principles calculations. In both complexes, the main anisotropy axis is along the N2–N3 direction (see Figure 2) and is perpendicular to the pseudo-C_2 axis, which passes between O1 and O2 (Figure 8). It is useful to point out that, in most low-symmetry mononuclear dysprosium(III) complexes, the ground Kramers doublet may be best described as $|J = {}^{15}/_2, M_J = {}^{15}/_2\rangle$, with the **g** tensor approaching 20. With this approximation, it is possible to successfully use an electrostatic model to determine the orientation of the anisotropy axis.[12k,38] However, this method does not give access to the value of the **g** tensor, which is crucial in determining the nature of the Kramers doublets.

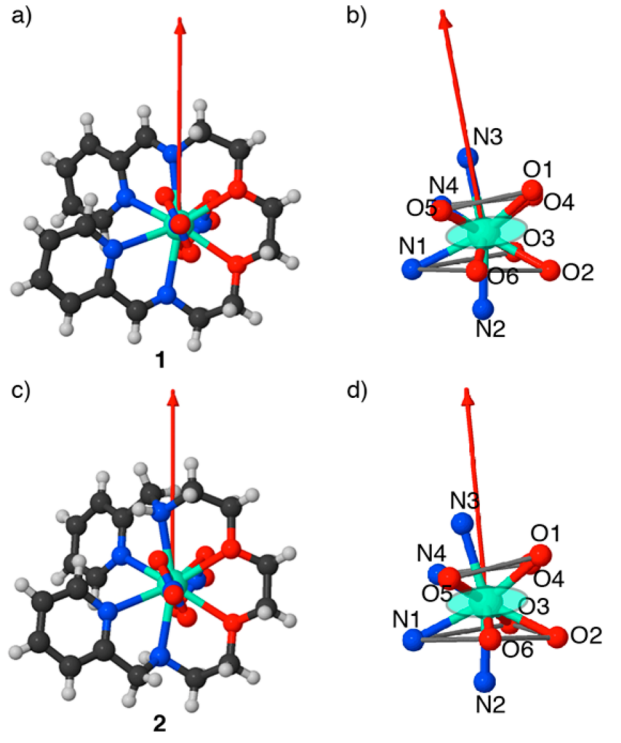

Figure 8. Orientations of the main magnetic axis for **1** (a and b) and **2** (c and d). Green oval: graphical representation of the oblate f-electron charge cloud of the dysprosium(III) ions oriented according to the anisotropy axis.

dx.doi.org/10.1021/ic402950j | Inorg. Chem. 2014, 53, 2598–2605

Because it is possible to mathematically approximate the quadrupole moment of the f-electron charge cloud of dysprosium(III) ions as oblate (for $M_J = {}^{15}/_{2}$),[8a] it is therefore possible to say that an optimal crystal field, which would stabilize the larger M_J sublevels and thus lead to highly anisotropic molecules, should be placed above and below the *xy* plane, which is along the main anisotropy axes determined from first-principles calculations. Thus, in our system, the position of the donor atoms with respect to the main magnetic axes is almost identical with the above description. Therefore, it was reasoned that the differences in the magnetic anisotropy observed between **1** and **2** were also a consequence of contributions from the ligand donor atoms. Similar to that observed by Murugesu and co-workers, where a decreased electron density along the hard axis also leads to a more anisotropic dysprosium(III) ion, and supported by Long et al., we reason that the difference in the values of the energy barrier of reorientation of the magnetization was given by two factors. First, the shorter imine bonds, at the N2 and N3 positions, lead to stronger bonds in the axial position and, thus, a stronger overall ligand field. Second, the increased electron density in the easy plane (along the anisotropy axis) results in a more anisotropic dysprosium(III) ion and, therefore, in a complex with a larger barrier of reorientation of the magnetization.

Thus, changing the donor atoms within a ligand system affects the electron density and therefore the overall magnetic behavior of the resulting isostructural complexes.

CONCLUSIONS

In conclusion, we have shown how a small modification in the ligand system results in the synthesis of two isostructural compounds that have different magnetic properties. The observed differences in the magnetic data were validated by first-principles calculations, which indicated that the two complexes have different values for the energy gap of the first excited states and different *g* factors, leading to different low-lying ground-state Kramers doublets. These differences were attributed not only to the coordination geometry, which is almost identical in the two complexes, but also to the nature of the donor atoms. All but two (N1 and N2) of the 10 donor atoms are identical. The main difference arises because the ligand field (the electron density) of two of the nitrogen atoms differs because imine nitrogen atoms (**1**) give rise to a stronger ligand field than amine nitrogen atoms (**2**). The stronger ligand field possesses a larger electron density and results in a complex (**1**) with a larger energy difference between the ground state and first excited state and therefore in a larger magnetic anisotropy of the ground state, which directly translated to a larger energy barrier of reorientation of the magnetization. This system may be seen as a stepping stone upon which other model systems might be built upon in order to generate a set of "chemical" rules that govern SMM assembly and control.

ASSOCIATED CONTENT

Supporting Information

Crystallographic data in CIF format (CCDC 911884 and 918341), magnetic data, and theoretical calculations. This material is available free of charge via the Internet at http://pubs.acs.org.

AUTHOR INFORMATION

Corresponding Authors

*E-mail: victoria.campbell@u-psud.fr.

*E-mail: talal.mallah@u-psud.fr.

Author Contributions

The manuscript was written through contributions of all authors. All authors have given approval to the final version of the manuscript.

Notes

The authors declare no competing financial interest.

ACKNOWLEDGMENTS

This work is partially financed by ANR-project MolNanoSpin No. ANR-08-NANO-002, ANR-09-BLAN-0195-TEMAMA, and ERC Advanced Grant MolNanoSpin No. 226558. T.M. thanks the Institut Universitaire de France for financial support.

REFERENCES

(1) Jones, N. *Nature (London, U. K.)* **2011**, *472*, 22−23.

(2) (a) Caneschi, A.; Gatteschi, D.; Sessoli, R.; Barra, A. L.; Brunel, L. C.; Guillot, M. *J. Am. Chem. Soc.* **1991**, *113*, 5873−5874. (b) Moragues-Canovas, M.; Helliwell, M.; Ricard, L.; Riviere, E.; Wernsdorfer, W.; Brechin, E.; Mallah, T. *Eur. J. Inorg. Chem.* **2004**, 2219−2222.

(3) Gatteschi, D.; Sessoli, R.; Villain, J. *Molecular Nanomagnets*; Oxford University Press: Oxford, U.K., 2006.

(4) (a) Sessoli, R.; Tsai, H. L.; Schake, A. R.; Wang, S.; Vincent, J. B.; Folting, K.; Gatteschi, D.; Christou, G.; Hendrickson, D. N. *J. Am. Chem. Soc.* **1993**, *115*, 1804−1816. (b) Sessoli, R.; Gatteschi, D.; Caneschi, A.; Novak, M. A. *Nature* **1993**, *365*, 141−143.

(5) (a) Chakov, N. E.; Lee, S.-C.; Harter, A. G.; Kuhns, P. L.; Reyes, A. P.; Hill, S. O.; Dalal, N. S.; Wernsdorfer, W.; Abboud, K. A.; Christou, G. *J. Am. Chem. Soc.* **2006**, *128*, 6975−6989. (b) Milios, C. J.; Vinslava, A.; Wernsdorfer, W.; Moggach, S.; Parsons, S.; Perlepes, S. P.; Christou, G.; Brechin, E. K. *J. Am. Chem. Soc.* **2007**, *129*, 2754−2755.

(6) Urdampilleta, M.; Klyatskaya, S.; Cleuziou, J.-P.; Ruben, M.; Wernsdorfer, W. *Nat. Mater.* **2011**, *10*, 502−506.

(7) (a) Wang, X.-Y.; Avendaño, C.; Dunbar, K. R. *Chem. Soc. Rev.* **2011**, *40*, 3213−3238. (b) Rinehart, J. D.; Fang, M.; Evans, W. J.; Long, J. R. *J. Am. Chem. Soc.* **2011**, *133*, 14236−14239. (c) Rinehart, J. D.; Fang, M.; Evans, W. J.; Long, J. R. *Nat. Chem.* **2011**, *3*, 538−542.

(8) (a) Rinehart, J. D.; Long, J. R. *Chem. Sci.* **2011**, *2*, 2078−2085. (b) Sessoli, R.; Powell, A. K. *Coord. Chem. Rev.* **2009**, *253*, 2328−2341. (c) Zaleski, C. M.; Depperman, E. C.; Kampf, J. W.; Kirk, M. L.; Pecoraro, V. L. *Angew. Chem., Int. Ed.* **2004**, *43*, 3912−3914. (d) Luzon, J.; Sessoli, R. *Dalton Trans.* **2012**, *41*, 13556−13567. (e) Langley, S. K.; Wielechowski, D. P.; Vieru, V.; Chilton, N. F.; Moubaraki, B.; Abrahams, B. F.; Chibotaru, L. F.; Murray, K. S. *Angew. Chem., Int. Ed.* **2013**, *52*, 12014−12019. (f) Meihaus, K. R.; Long, J. R. *J. Am. Chem. Soc.* **2013**, *135*, 17952−17957. (g) Le Roy, J. J.; Jeletic, M.; Gorelsky, S. I.; Korobkov, I.; Ungur, L.; Chibotaru, L. F.; Murugesu, M. *J. Am. Chem. Soc.* **2013**, *135*, 3502−3510.

(9) (a) Blagg, R. J.; Muryn, C. A.; McInnes, E. J. L.; Tuna, F.; Winpenny, R. E. P. *Angew. Chem., Int. Ed.* **2011**, *50*, 6530−6533. (b) Blagg, R. J.; Ungur, L.; Tuna, F.; Speak, J.; Comar, P.; Collison, D.; Wernsdorfer, W.; McInnes, E. J. L.; Chibotaru, L. F.; Winpenny, R. E. P. *Nat. Chem.* **2013**, *5*, 673−678.

(10) Ishikawa, N.; Sugita, M.; Ishikawa, T.; Koshihara, S.-y.; Kaizu, Y. *J. Am. Chem. Soc.* **2003**, *125*, 8694−8695.

(11) AlDamen, M. A.; Clemente-Juan, J. M.; Coronado, E.; Martí-Gastaldo, C.; Gaita-Ariño, A. *J. Am. Chem. Soc.* **2008**, *130*, 8874−8875.

(12) (a) Long, J.; Habib, F.; Lin, P.-H.; Korobkov, I.; Enright, G.; Ungur, L.; Wernsdorfer, W.; Chibotaru, L. F.; Murugesu, M. *J. Am. Chem. Soc.* **2011**, *133*, 5319−5328. (b) Habib, F.; Murugesu, M. *Chem. Soc. Rev.* **2013**, *42*, 3278−3288. (c) Woodruff, D. N.; Winpenny, R. E. P.; Layfield, R. A. *Chem. Rev.* **2013**, 5110−5148. (d) Zheng, Y.-Z.; Lan, Y.; Anson, C. E.; Powell, A. K. *Inorg. Chem.* **2008**, *47*, 10813−10815. (e) Campbell, V. E.; Guillot, R.; Rivière, E.; Brun, P.-T.; Wernsdorfer, W.; Mallah, T. *Inorg. Chem.* **2013**, *52*, 5194−5200. (f) Bhunia, A.;

Gamer, M. T.; Ungur, L.; Chibotaru, L. F.; Powell, A. K.; Lan, Y.; Roesky, P. W.; Menges, F.; Riehn, C.; Niedner-Schatteburg, G. *Inorg. Chem.* **2012**, *51*, 9589−9597. (g) Feltham, H. L. C.; Clérac, R.; Ungur, L.; Chibotaru, L. F.; Powell, A. K.; Brooker, S. *Inorg. Chem.* **2013**, *52*, 3236−3240. (h) Lin, P.-H.; Burchell, T. J.; Clérac, R.; Murugesu, M. *Angew. Chem., Int. Ed.* **2008**, *47*, 8848−8851. (i) Westerström, R.; Dreiser, J.; Piamonteze, C.; Muntwiler, M.; Weyeneth, S.; Brune, H.; Rusponi, S.; Nolting, F.; Popov, A.; Yang, S.; Dunsch, L.; Greber, T. *J. Am. Chem. Soc.* **2012**, *134*, 9840−9843. (j) Boulon, M.-E.; Cucinotta, G.; Luzon, J.; Degl'Innocenti, C.; Perfetti, M.; Bernot, K.; Calvez, G.; Caneschi, A.; Sessoli, R. *Angew. Chem., Int. Ed.* **2012**, *52*, 350−354. (k) Chilton, N. F.; Langley, S. K.; Moubaraki, B.; Soncini, A.; Batten, S. R.; Murray, K. S. *Chem. Sci.* **2013**, *4*, 1719−1730. (l) Fortea-Pérez, F. R.; Vallejo, J.; Julve, M.; Lloret, F.; De Munno, G.; Armentano, D.; Pardo, E. *Inorg. Chem.* **2013**, *52*, 4777−4779.

(13) AlDamen, M. A.; Cardona-Serra, S.; Clemente-Juan, J. M.; Coronado, E.; Gaita-Ariño, A.; Martí-Gastaldo, C.; Luis, F.; Montero, O. *Inorg. Chem.* **2009**, *48*, 3467−3479.

(14) (a) Ishikawa, N.; Sugita, M.; Wernsdorfer, W. *Angew. Chem., Int. Ed.* **2005**, *44*, 2931−2935. (b) Feltham, H. L. C.; Clérac, R.; Ungur, L.; Vieru, V.; Chibotaru, L. F.; Powell, A. K.; Brooker, S. *Inorg. Chem.* **2012**, *51*, 10603−10612. (c) Baldoví, J. J.; Cardona-Serra, S.; Clemente-Juan, J. M.; Coronado, E.; Gaita-Ariño, A.; Palii, A. *Inorg. Chem.* **2012**, *51*, 12565−12574.

(15) Habib, F.; Long, J.; Lin, P.-H.; Korobkov, I.; Ungur, L.; Wernsdorfer, W.; Chibotaru, L. F.; Murugesu, M. *Chem. Sci.* **2012**, *3*, 2158−2164.

(16) Tanaka, D.; Inose, T.; Tanaka, H.; Lee, S.; Ishikawa, N.; Ogawa, T. *Chem. Commun.* **2012**, *48*, 7796−7798.

(17) Habib, F.; Brunet, G.; Vieru, V.; Korobkov, I.; Chibotaru, L. F.; Murugesu, M. *J. Am. Chem. Soc.* **2013**, *135*, 13242−13245.

(18) (a) Jubert, C.; Mohamadou, A.; Marrot, J.; Barbier, J.-P. *J. Chem. Soc., Dalton Trans.* **2001**, 1230−1238. (b) Arulsamy, N.; Glerup, J.; Hazell, A.; Hodgson, D. J.; McKenzie, C. J.; Toftlund, H. *Inorg. Chem.* **1994**, *33*, 3023−3025.

(19) Sheldrick, G. M. *SHELXS-97, Program for Crystal Structure Solution*; University of Göttingen: Göttingen, Germany, 1997.

(20) Sheldrick, G. M. *SHELXL-97, Program for the refinement of crystal structures from diffraction data*; University of Göttingen: Göttingen, Germany, 1997.

(21) Farrugia, L. J. *J. Appl. Crystallogr.* **1999**, 837−838.

(22) Wernsdorfer, W. *Supercond. Sci. Technol.* **2009**, *22*, 064013.

(23) Kahn, O. *Molecular Magnetism*; VCH: Weinheim, Germany, 1993.

(24) (a) Gamer, M. T.; Lan, Y.; Roesky, P. W.; Powell, A. K.; Clérac, R. *Inorg. Chem.* **2008**, *47*, 6581−6583. (b) Layfield, R. A.; McDouall, J. J. W.; Sulway, S. A.; Tuna, F.; Collison, D.; Winpenny, R. E. P. *Chem.—Eur. J.* **2010**, *16*, 4442−4446.

(25) Hill, S.; Datta, S.; Liu, J.; Inglis, R.; Milios, C. J.; Feng, P. L.; Henderson, J. J.; del Barco, E.; Brechin, E. K.; Hendrickson, D. N. *Dalton Trans.* **2010**, *39*, 4693−4707.

(26) Kramers, H. A. *Proc. K. Ned. Akad. Wet.* **1930**, *33*, 959−972.

(27) Wernsdorfer, W.; Bhaduri, S.; Boskovic, C.; Christou, G.; Hendrickson, D. *Phys. Rev. B* **2002**, *65*, 180403.

(28) Car, P.-E.; Perfetti, M.; Mannini, M.; Favre, A.; Caneschi, A.; Sessoli, R. *Chem. Commun.* **2011**, *47*, 3751−3753.

(29) Feltham, H. L. C.; Lan, Y.; Klöwer, F.; Ungur, L.; Chibotaru, L. F.; Powell, A. K.; Brooker, S. *Chem.—Eur. J.* **2011**, *17*, 4362−4365.

(30) (a) Cole, K. S.; Cole, R. H. *J. Chem. Phys.* **1941**, *9*, 341−351. (b) Miyasaka, H.; Clérac, R.; Mizushima, K.; Sugiura, K.-i.; Yamashita, M.; Wernsdorfer, W.; Coulon, C. *Inorg. Chem.* **2003**, *42*, 8203−8213.

(31) Ishikawa, N. *J. Phys. Chem. A* **2003**, *107*, 5831−5835.

(32) Aravena, D.; Ruíz, E. *Inorg. Chem.* **2013**, *52*, 13770−13778.

(33) (a) Aquilante, F.; De Vico, L.; Ferrã, N.; Ghigo, G.; Malmqvist, P.-Ã. k.; Neogrãdy, P.; Pedersen, T. B.; Pitonìãk, M.; Reiher, M.; Roos, B. r. O.; Serrano-Andrãs, L.; Urban, M.; Veryazov, V.; Lindh, R. *J. Comput. Chem.* **2010**, *31*, 224−247. (b) Ungur, L.; Van den Heuvel, W.; Chibotaru, L. F. *New J. Chem.* **2009**, *33*, 1224−1230.

(34) Roos, B. O.; Taylor, P. R.; Siegbahn, E. M. *Chem. Phys.* **1980**, *48*, 157−173.

(35) Malmqvist, P. A.; Roos, B. O.; Schimmelpfennig, B. *Chem. Phys. Lett.* **2002**, *357*, 230−240.

(36) Bolvin, H. *ChemPhysChem* **2006**, *7*, 1575−1589.

(37) Høg, J.; Touborg, P. *Phys. Rev. B* **1975**, *11*, 520−529.

(38) Chilton, N. F.; Collison, D.; McInnes, E. J. L.; Winpenny, R. E. P.; Soncini, A. *Nat. Commun.* **2013**, *4*, 1−7.